



# Methylation of ciliary dynein motors involves the essential cytosolic assembly factor DNAAF3/PF22

Miho Sakato-Antoku<sup>a</sup> , Ramila S. Patel-King<sup>a</sup>, Jeremy L. Balsbaugh<sup>b</sup> , and Stephen M. King<sup>a,1</sup>

Edited by Mary E. Porter, University of Minnesota Twin Cities, Minneapolis, MN; received October 23, 2023; accepted December 15, 2023  
by Editorial Board Member Yale E. Goldman

**Axonemal dynein motors drive ciliary motility and can consist of up to twenty distinct components with a combined mass of ~2 MDa.** In mammals, failure of dyneins to assemble within the axonemal superstructure leads to primary ciliary dyskinesia. Syndromic phenotypes include infertility, rhinitis, severe bronchial conditions, and situs inversus. Nineteen specific cytosolic factors (Dynein Axonemal Assembly Factors; DNAAFs) are necessary for axonemal dynein assembly, although the detailed mechanisms involved remain very unclear. Here, we identify the essential assembly factor DNAAF3 as a structural ortholog of S-adenosylmethionine-dependent methyltransferases. We demonstrate that dynein heavy chains, especially those forming the ciliary outer arms, are methylated on key residues within various nucleotide-binding sites and on microtubule-binding domain helices directly involved in the transition to low binding affinity. These variable modifications, which are generally missing in a *Chlamydomonas* null mutant for the DNAAF3 ortholog PF22 (DAB1), likely impact on motor mechanochemistry fine-tuning the activities of individual dynein complexes.

axoneme | *Chlamydomonas* | cilia | dynein | microtubule

Dyneins are highly complex molecular motors that mediate transport toward the minus end of microtubules (see various chapters in ref. 1). Dedicated dyneins function to move cargos in the cytoplasm and to power retrograde intraflagellar transport (IFT) in cilia. Numerous other dyneins are arrayed in a complex pattern along the ciliary length (2) and generate rhythmic beating of these organelles; this can propel individual cells or move fluids across surfaces. Defects in axonemal dynein proteins themselves or in many of their cytoplasmic assembly factors lead to primary ciliary dyskinesia in humans (3, 4). This syndrome can involve male and female infertility, severe bronchial problems, chronic rhinitis, otitis media, hydrocephalus, and incorrect assignment of the left-right body axis (5). Abnormal dynein-driven ciliary motility has also been linked to congenital heart disease (6) and various forms of epilepsy, e.g., refs. 7 and 8.

Dyneins are built around the ~540-kDa heavy chains (HCs), which contain an N-terminal region involved in inter-HC associations and axonemal docking, followed by a linker domain that moves during the power stroke and crosses a hexameric ring of six different AAA<sup>+</sup> units (AAA1-6) (9–13). The microtubule-binding domain is located at the tip of an antiparallel coiled-coil stalk that derives from AAA4 and is supported by a second coiled coil from AAA5. Changes in coiled-coil registry driven by adenosine 5'-triphosphate (ATP) binding, hydrolysis, and product release at AAA1 lead to alterations in microtubule-binding affinity (14). Binding of nucleotides at AAA2-AAA4 acts to modify the dynein mechanochemical cycle (15). Dyneins also contain a series of other components involved in formation of the holoenzymes, cargo binding, and motor regulation. For example, the outer arm dynein from the green alga *Chlamydomonas reinhardtii* consists of three distinct HCs (termed α, β, and γ), two intermediate chains (ICs), and ten different light chains (LCs) with a combined total mass of ~2 MDa and associates with a trimeric docking complex needed for axonemal incorporation (16).

Assembly of axonemal dyneins occurs in the cytoplasm and the fully formed motors are then trafficked to and inserted into the axonemal superstructure within a 96-nm repeating unit that consists of four outer arms, one inner arm I1/f with two motor units and six different inner arm dyneins containing single HCs (17, 18). This cytoplasmic assembly process is highly complex. Each HC mRNA is ~15 kb and ribosomes, which function at ~5 residues/s, take almost 15 min to synthesize these ~4,500-residue HC proteins (19). As HCs have a circular arrangement of AAA<sup>+</sup> domains, they do not form a stable folded structure until after AAA6 has been synthesized thereby completing the hexameric ring. Other dynein components must associate with the nascent HCs to ultimately generate the holoenzyme. In addition to ribosomes, various chaperones, prefoldins,

## Significance

Axonemal dyneins power ciliary motility moving individual cells and generating fluid flows. In humans, loss of cilia-driven locomotion leads to infertility, severe bronchial problems, situs inversus, and other phenotypes. Dyneins are preassembled in the cytoplasm before being trafficked into the cilium. At least nineteen specific factors are necessary for axonemal dynein formation; however, the mechanisms involved remain very poorly understood. Here, we identify the assembly factor DNAAF3/PF22 as an S-adenosylmethionine-dependent methyltransferase. Furthermore, we find that dyneins are methylated on key arginine and lysine residues within the ATP- and microtubule-binding domains which will affect motor properties. These extensive modifications add an additional level of complexity to the analysis of native dynein proteins as they exist as an array of variably methylated types.

Author contributions: J.L.B. and S.M.K. designed research; M.S.-A., R.S.P.-K., and J.L.B. performed research; J.L.B. and S.M.K. analyzed data; and M.S.-A., R.S.P.-K., J.L.B., and S.M.K. wrote the paper.

The authors declare no competing interest.

This article is a PNAS Direct Submission. M.E.P. is a guest editor invited by the Editorial Board.

Copyright © 2024 the Author(s). Published by PNAS. This article is distributed under Creative Commons Attribution-NonCommercial-NoDerivatives License 4.0 (CC BY-NC-ND).

<sup>1</sup>To whom correspondence may be addressed. Email: king@uchc.edu.

This article contains supporting information online at <https://www.pnas.org/lookup/suppl/doi:10.1073/pnas.2318522121/-DCSupplemental>.

Published January 23, 2024.

and the RuvBL1/2 ATPases, nineteen cytosolic factors (DNAAFs) have been identified as specifically involved in axonemal dynein formation (see ref. 20 for a listing and updated nomenclature). Studies in vertebrate multiciliated cells suggest that axonemal dynein assembly occurs within cytosolic, possibly phase-separated, compartments (21). Furthermore, although many individual assembly factors contain protein interaction modules and inherently disordered regions, their precise role(s) and the detailed mechanisms by which these enormous complexes are built in the cytoplasm prior to their transport into growing cilia remain very unclear (17, 19, 22).

The axonemal dynein assembly factor designated as DNAAF3 (*Homo*), Dnaaf3 (*Danio* and *Drosophila*), and PF22 (also termed DAB1 (23); *Chlamydomonas*) is directly involved in HC formation in cytoplasm and its dysfunction leads to loss of outer dynein arms and some or all inner dynein arms in cilia of *Chlamydomonas*, zebrafish and humans (24) and *Drosophila* (25), resulting in primary ciliary dyskinesia in humans (24). Here, we find that DNAAF3 is a structural relative of S-adenosylmethionine (SAM)-dependent methyltransferases. Using mass spectrometry (MS/MS), we identify numerous sites of mono-/dimethylation of arginine and mono-/di-/trimethylation of lysine residues within dynein HCs; axonemal dynein proteins obtained from the cytoplasm of a *Chlamydomonas* null mutant for the DNAAF3 ortholog PF22 (24, 26) generally lack these modifications. Many methylated sites occur on key residues within the ATP- and microtubule-binding domains of outer and inner arm dynein HCs and the IFT dynein HC. Methylation has major effects on the chemistry of basic residues increasing their bulk and hydrophobicity, reducing H bond capacity, and delocalizing the +1 charge across adjacent hydrocarbon groups (27, 28) (*SI Appendix*, Fig. S1). Consequently, these modifications may represent a posttranslational mechanism fine-tuning the activity of individual dynein HC motors.

## Results

**DNAAF3/PF22 Is Structurally Related to S-Adenosylmethionine-Dependent Methyltransferases.** To obtain insight into the cytoplasmic mechanisms of axonemal dynein assembly, we examined the AlphaFold2 predictions for all nineteen currently identified assembly factors (DNAAFs) from human, mouse, rat, zebrafish and *Chlamydomonas*; all vertebrate model structures were downloaded from UniProt (<https://www.uniprot.org/>) while the *Chlamydomonas* predictions were generated using the ColabFold server (29). Several of these proteins (e.g., DNAAF1/LRRC50, DNAAF4/DYX1C1, and DNAAF5/HEATR2) consist of protein–protein interaction modules in several cases combined with large unstructured regions (17, 20, 22). Others contain PIH domains, which associate with the R2TP complex and its variants to recruit heat shock proteins (e.g., DNAAF2/PF13, DNAAF6/PIH1D3, DNAAF14/PIH1D1, and DNAAF15/PIH1D2) (30), whereas DNAAF8/C16orf71, for example, has little or no predicted tertiary structure (22). However, the prediction for DNAAF3 was distinct. The arrangement of secondary structural elements (Fig. 1A) indicates that it is based on a variation of the Rossmann fold that classically consists of a β sheet containing six parallel strands formed from two β-β-β motifs and which often bind nucleotide-based cofactors such as FAD and NADH (31). Rossmann fold-based enzymes frequently include a seventh antiparallel strand in the sequence 3-2-1-4-5-7-6 (32); for DNAAF3, the antiparallel strand is present; however, AlphaFold2 does not predict the sixth strand but rather a loop region. This N-terminal α/β globular domain contains a relatively deep cleft on one face and is followed by a C-terminal disordered segment (Fig. 1B and C).

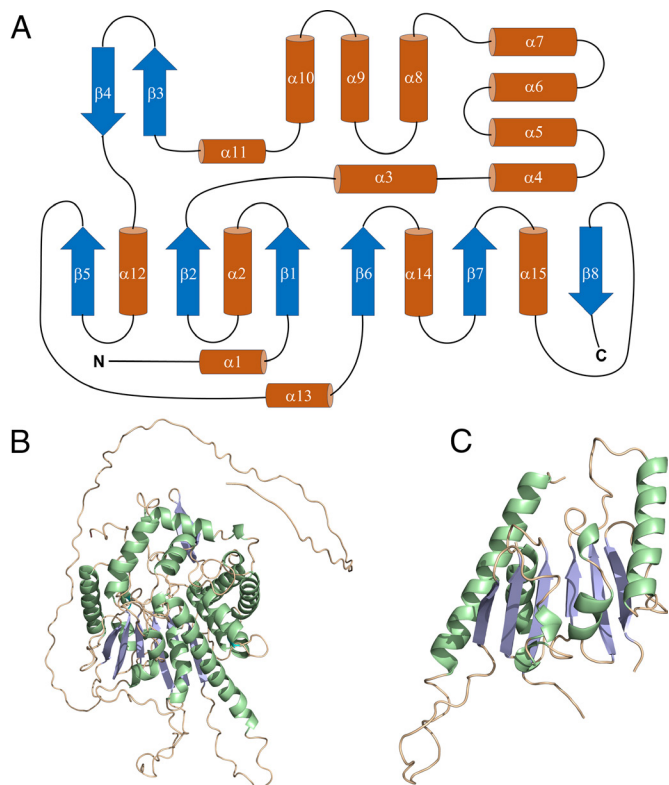


**Fig. 1.** DNAAF3 is built on a Rossmann fold. (A) Diagram illustrating the secondary structure organization of human DNAAF3. Rossmann folds usually consist of two β-α-β-α-β motifs forming a six-stranded parallel β sheet. For DNAAF3, the sixth strand is not predicted, and an antiparallel seventh strand often seen in Rossmann fold variants is present. A large subdomain consisting of nine helices and a β hairpin connects stand β2 and helix α12 in the Rossmann fold. (B) Ribbon diagram of the AlphaFold2 prediction for full-length human DNAAF3; helices, light green; strands, light blue; loops, wheat. The C-terminal region is inherently disordered. (C) Ribbon diagram of the elements comprising the Rossmann fold; the subdomain consisting of helices α3-α11 and strands β3 and β4 has been hidden for clarity.

We then used DALI (33) to search the Protein Data Bank (PDB) (<https://www.rcsb.org/>) for structurally related proteins. AlphaFold2 predictions for the globular domains of human DNAAF3, zebrafish Dnaaf3, and *Chlamydomonas* PF22 all identified long lists of structural homologs functionally annotated as SAM-dependent methyltransferases (Dataset S1). These structural alignments with DNAAF3 orthologs have rmsds of ~2.4 to 3.5 Å covering ~140 or more residues with z scores in many cases >10; a score of  $z = 6$  is generally considered highly significant, while a score of  $z \leq 2$  is meaningless (Fig. 2 A–C). Importantly, many of the aligned experimental structures were solved with the S-adenosylhomocysteine (SAH) methylation by-product in the active site (Fig. 2 A–D); this revealed that the structural alignments with DNAAF3 and PF22 are centered on the methyltransferase region directly involved in binding SAM (Fig. 2 A–C).

Two structural features have been identified as key to SAM binding by Rossmann fold-based methyltransferases: a Gly-rich loop connecting the first β strand and α helix, and an acidic residue at the end of the second β strand that makes bidentate interactions with the ribose hydroxyls of SAM (32). Both features are present in DNAAF3 orthologs (Fig. 2C). Although there is variation in the Gly-rich loop sequences from the canonical xGxG consensus in some DNAAF3 proteins (e.g., GxxxG in human DNAAF3 compared to GGGxG in *Xenopus* and even AxxxA in *Chlamydomonas*), the AlphaFold2-modeled backbone orientations are similar to those observed in the experimentally determined methyltransferase structures (Fig. 2C). Given the alignment

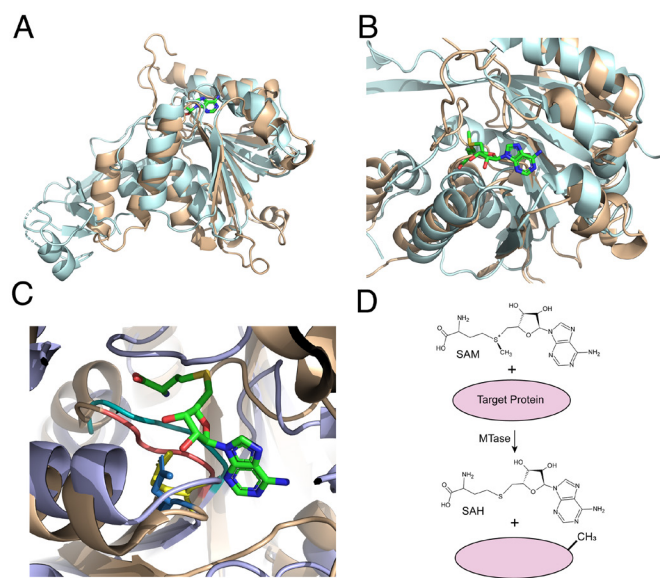


**Fig. 2.** Structural orthology of DNAAF3 and PF22 with methyltransferases. (A) Structural overlay of the *Chlamydomonas* PF22 AlphaFold2 model (pale cyan) with the X-ray crystal structure of the Trm1 tRNA methylase from *Thermus thermophila* [light orange; PDB accession 5C00 (34)]; this alignment is over 145 residues (19% sequence identity) with an rmsd of 2.5 Å and a z score of 9.5. The SAH methylation by-product within the methyltransferase active site is shown colored by element (C, green; N, blue; O, red; S, yellow). (B) Magnified view of the SAM binding site of Trm1 with PF22 overlaid. (C) Close-up view of SAH in the active site of the methyltransferase 2 domain of the AprA polyketide synthase from the cyanobacterium *Moerella bouillonii* [light blue; PDB accession 6D6Y (35)] with the human DNAAF3 AlphaFold2 model (light orange) overlaid. The Gly-rich loop (teal and deep salmon, respectively) that forms the base of the SAM/SAH binding pocket and the acidic residue (yellow and sky blue, respectively) at the end of the second β strand in the Rossmann fold that makes bidentate interactions with the ribose hydroxyls are shown. (D) The general reaction catalyzed by SAM-dependent methyltransferases (MTase). The methyl group attached to the sulfonium ion of SAM is transferred directly to the target protein side chain resulting in the methylated product and demethylated SAH.

parameters, these structural relationships are likely significant even though the level of primary sequence conservation between the aligned segments of annotated methyltransferases and DNAAF3 orthologs is generally low (<20% sequence identity). A contrastive machine learning model that predicts enzyme function from primary sequence (36) also suggests that human DNAAF3 and *Chlamydomonas* PF22 may be SAM-dependent type II protein arginine methyltransferases (enzyme commission # EC 2.1.1.320); these generate monomethyl and symmetric dimethyl arginine.

**Methylation of Axonemal Dynein HCs on Arginine and Lysine Residues.** Identification of DNAAF3 as structurally related to methyltransferases prompted us to ask whether dyneins and specifically the HC motor units are modified in this manner. Initially, we re-searched the raw data from a previous MS/MS analysis of *Chlamydomonas* cilia (37) for monomethylation and found numerous instances of modified Arg/Lys residues within axonemal dynein HCs from replicate samples; in contrast, there was little evidence for other dynein components being methylated.

We then examined dynein HCs electrophoretically purified from wild-type axonemes (Fig. 3A) to more fully explore these observations and obtain greater sequence coverage, searching for all possible modes of Arg/Lys methylation in multiple biological replicates digested with either trypsin or endoproteinase AspN and processed at different times; we also analyzed an axonemal sample prepared from the *oda2* mutant which only assembles inner arm dyneins in an attempt to obtain better sequence coverage of

some minor inner arm HCs. This identified a series of basic residues within axonemal dynein HCs that are subject to methylation (Dataset S2 and SI Appendix, Table S1) for the properties and locations of all identified methylated residues). The number of modified residues per HC varied from ~1 to 6% of the total number present in the primary sequence; total relative abundance of each methylation posttranslational modification varies, with the outer arm α and β HCs being most heavily alkylated (Table 1).

Sequence alignments revealed a significant degree of specificity to the modifications (Dataset S2). For example, although the α and β HCs have very distinct ~1,000 residue N-terminal domains, their motor units are paralogous (38). Of the thirty-five methylated sites found throughout the β HC, the corresponding residue

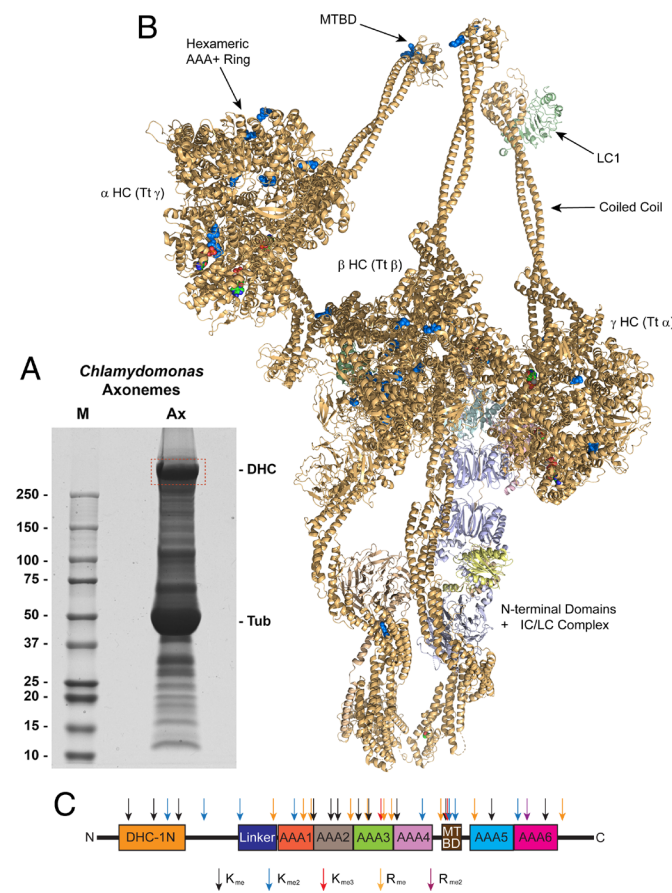


**Fig. 3.** Location of methylated residues within outer arm dynein. (A) Ciliary axonemes obtained from CC-125 wild-type cells were electrophoresed to separate the dynein HCs (labeled DHC) from most other axonemal components. The HC band (area boxed by red dashed line) was excised and subject to mass spectrometric analysis. (B) Methylated Arg/Lys residues identified in *Chlamydomonas* outer arm dynein HCs were mapped onto the cryo-electron microscopy structure of *Tetrahymena* outer arm dynein [PDB 7KEK; (12)] and displayed as space-filling side chains in marine blue; only residues where a basic amino acid is conserved between the two species are highlighted. For historical reasons (23), axonemal HC nomenclature is confusing: here, although the β HCs are equivalent between these species, the *Chlamydomonas* α and γ HCs are orthologous to the *Tetrahymena* γ and α HCs, respectively. Therefore, to avoid confusion with the rest of the text, the HCs in this diagram are indicated using the *Chlamydomonas* nomenclature with the *Tetrahymena* name in parentheses, e.g., α HC (Tt γ). Methylated sites on basic residues conserved between *Chlamydomonas* and *Tetrahymena* mainly cluster in the AAA domains and MTBDs of the α and β HCs. Locations of various HC regions, the IC/LC complex, and the LC1 protein associated with the MTBD of the γ HC (Tt α) are indicated. This ribbon structure was drawn using ray tracing within PyMOL (and Movie S1). (C) Map of the 4,568-residue β HC from *Chlamydomonas* outer arm dynein indicating the location of methylated sites; where a residue was found in several different modification states, the most highly methylated form is indicated.

**Table 1. Overall dynein heavy chain methylation parameters\***

Dynein heavy chain	Total residues (n)	Total K+R residues (n)	Lysine (n)			Arginine (n)		Number of K/R residues modified (n; %)
			Monomethyl	Dimethyl	Trimethyl	Monomethyl	Dimethyl <sup>†</sup>	
DHC13 (OAD $\alpha$ )	4,503	506	7	1	1	21	1	31; 6.1
DHC14 (OAD $\beta$ )	4,568	550	12	9	2	11	1	35; 6.4
DHC15 (OAD $\gamma$ )	4,501	562	6	0	1	7	1	15; 2.7
DHC1 (IAD I1/f 1 $\alpha$ )	4,625	646	4	0	1	2	1	8; 1.4
DHC10 (IAD I1/f 1 $\beta$ )	4,513	559	5	1	2	4	0	12; 2.6
DHC9 (IAD c)	4,151	478	8	0	0	3	0	11; 2.2
DHC11 (IAD minor)	4,757	487	2	0	1	1	2	6; 1.2
DHC16 (IFT) <sup>‡</sup>	4,333	510	4	0	1	3	0	8; 1.6
Dync1h1 (Rat Cytoplasmic) <sup>‡</sup>	4,644	586	1	0	0	1	0	2; 0.3

\*These values represent a compilation of all identified methylated sites within the indicated dynein HCs from multiple independent experiments and both tryptic and endoproteinase AspN digests. See *SI Appendix, Table S1* for a comprehensive list of identified methylated residues in all axonemal dynein HCs.

<sup>†</sup>Our mass spectral data do not distinguish between symmetric and asymmetric dimethylation of the arginine guanidinium group.

<sup>‡</sup>Intensities of methylated peptides from these related cytoplasmic dynein-like HCs were much lower than the unmodified forms.

in the  $\alpha$  HC was modified in nine cases, while the equivalent of methylated  $\beta$  HC residues R<sub>2332</sub> and K<sub>4114</sub> were modified in the IFT dynein, and in inner arm HCs I1  $\beta$  and DHC9, respectively. Detailed analysis of an additional, independently prepared, whole cilium sample again found no compelling evidence for any methyl modifications of non-HC dynein components.

### Modification of Nucleotide-Binding Sites in Dynein AAA+ Domains.

To gain broader insight into the potential impact of these modifications, we then mapped the identified methylated residues in *Chlamydomonas* outer arm dynein HCs onto the cryo-electron microscopy structure for the outer arm dynein from *Tetrahymena thermophila* [PDB 7KEK (12)]. This revealed that modifications mainly occur within the AAA domains of the outer arm motor units and on the MTBDs of the  $\alpha$  and  $\beta$ , but not  $\gamma$ , HCs (Fig. 3 B and C and Movie S1).

To assess how these modifications might affect nucleotide associations with individual dynein AAA+ domains we built AlphaFold2 models for several sections of the *Chlamydomonas*  $\beta$  HC and overlaid them on the cryo-electron microscopy structure of the human cytoplasmic dynein HC motor unit [5NUG 3.80 Å resolution; (39)] which was solved with ADP in AAA1, AAA3 and AAA4, and Mg-ATP in AAA2; alignment of AAA1+AAA2 regions of the two HCs for example has 33% sequence identity with an rmsd of 2.5 Å. Methylation sites that predictably might modify HC enzymology occur in three general locations—within the G(x)<sub>2</sub>G(x)GKT/S Walker A P-loop motifs of several AAA+ domains, in the WGCFDEFNR region of AAA1 that contains the Walker B box ( $\Phi$ )<sub>4</sub> DD/E (where  $\Phi$  is hydrophobic), and on the arginine fingers that derive from the following AAA+ domain and mediate inter-domain communication by detecting the nucleotide state of the preceding AAA+ domain and by stabilizing the transition state during hydrolysis; AAA+ domain ATPase sites lacking arginine fingers are generally inactive (e.g., the NSF D2 domain) (40, 41).

Within AAA1 of the outer arm  $\beta$  HC (Fig. 4 A and B), we identified monomethylation of R<sub>1975</sub> which is three residues from the Walker B box. This Arg residue is part of a highly conserved motif found in all dynein HCs and provides key interactions to orient one Walker B acidic sidechain within the active site. We also found that R<sub>2332</sub> (in the highly conserved PATVSR motif) which derives from AAA2 and provides the arginine finger in the

ATP hydrolytic site of AAA1 is methylated. This Arg residue is again dynein-invariant, and we identified this same modification, which might be expected to alter connectivity between domains, in the IFT dynein HC as well.

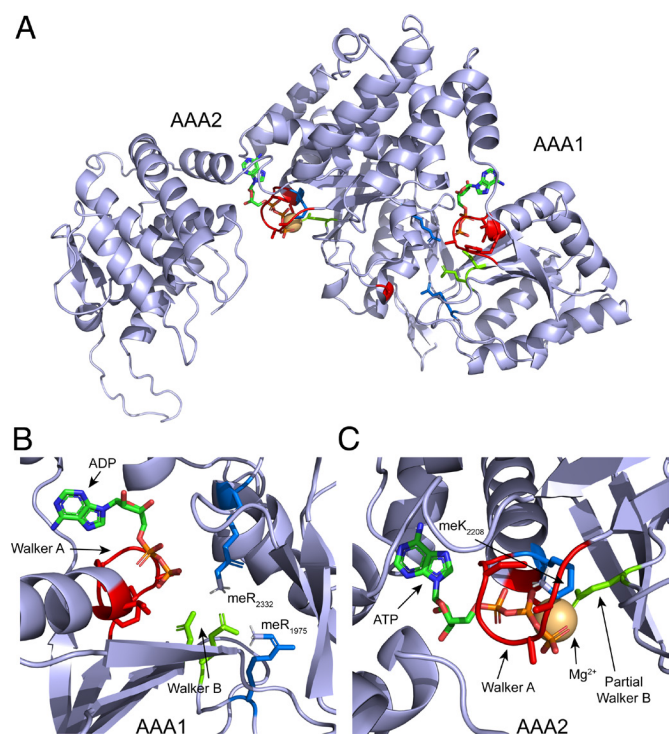


**Fig. 4.** Methylation of nucleotide binding domains in the  $\beta$  heavy chain. (A) Ribbon diagram of the AlphaFold2 model for AAA1+AAA2 of the outer arm  $\beta$  HC. Location of bound nucleotide was obtained by aligning this model with the human cytoplasmic dynein HC cryo-electron microscopy structure [5NUG 3.80 Å resolution; (39)] which was solved with ADP in AAA1 and Mg-ATP in AAA2. (B and C) Magnified views of the AAA1 and AAA2 nucleotide binding sites. In AAA1 (B), the dynein-invariant Arg residue downstream of the Walker B box (R<sub>1975</sub>) and the arginine finger (R<sub>2332</sub>) that derives from AAA2 are both methylated. In AAA2, the  $\beta$  HC is methylated on K<sub>2208</sub> within the Walker A P-loop motif. For all panels, the Walker A box is indicated in red, the Walker B acidic residues are in chartreuse, the Mg<sup>2+</sup> ion is wheat, and methylated basic residues are colored marine blue with the methyl group in silver/white.

The Walker B box is the primary driver of nucleotide hydrolysis and coordinates the Mg<sup>2+</sup> ion bound across the  $\beta$  and  $\gamma$  phosphates of ATP and orients the water molecule needed for hydrolysis. This metal ion together with a basic residue in the Walker A box that is directed toward the  $\gamma$ -phosphate acts to neutralize the high electronegativity of the triphosphate moiety sufficiently such that the  $\beta$ - $\gamma$  phospho-anhydride bond can be attacked by an incoming nucleophile. The AAA2 domain binds but does not hydrolyze ATP (42); generally, the Walker B box in AAA2 only contains the acidic residue that coordinates Mg<sup>2+</sup>. Within this  $\beta$  HC AAA2 region we find that the Lys residue in the Walker A box (Gx<sub>2</sub>GxGKT) is monomethylated (Fig. 4 A and C). This modification would generate a steric clash with the protein backbone of the Walker A box P-loop, place the triphosphate chain of ATP in a more hydrophobic environment, and partially delocalize the +1 charge on the sidechain thereby reducing its impact. When combined with loss of the second acidic residue within the Walker B box, this may be sufficient to completely inhibit nucleotide hydrolysis in AAA2 even though an arginine finger derived from AAA3 remains; intriguingly, within the outer arm  $\alpha$  HC, we found that this AAA3-derived arginine finger (R<sub>2500</sub>) oriented toward ATP bound in AAA2 is also monomethylated.

In addition, methylation of the Lys residue within the Walker A motif occurs in AAA3 of the IFT dynein HC (GPEGCGK G) and AAA4 of both the I1/f 1 $\alpha$  inner arm HC (GVGGSGKQ) and the IFT dynein HC (GNSGVGRR). It is noteworthy that modification of the equivalent residue in AAA1, which both binds and hydrolyzes ATP, was not found for any HC.

**Modified Dynein Microtubule-Binding Domains.** These small domains consist of ~100 residues forming six  $\alpha$  helices (H1 to H6; Fig. 5A) (14) and are located at the tip of an extended antiparallel coiled coil emanating from AAA4 (Fig. 3B). Movement of the first helix (H1) driven by changes in coiled-coil registry controls the transition between high- and low-affinity microtubule bound states. ATP binding at AAA1 leads to helix H1 pushing down on the microtubule and the ensuing steric clash with tubulin releases the high-affinity binding interface formed from helices H2, H3, H4, and H6 (43, 44).

We identified methylation of two regions within the MTBD (on helices H1 and H5), and several cases of modifications occurring along the extended coiled-coil region derived from AAA4 which undergoes an ATP-driven change in registry. The outer arm  $\alpha$  and  $\beta$  HCs and the I1/f 1 $\beta$  HC each contain three Lys residues in helix H1 arranged in a KK(D/E)X $\Phi$ E $\Phi$ K—hereafter KK(x)<sub>5</sub>K—motif that are variously modified leading to multiple distinct patterns identified by MaxQuant (Fig. 5 B–F). The fully unmodified forms of helix H1 were not identified for either the  $\alpha$  or  $\beta$  HCs, suggesting that all HCs of these types are methylated when incorporated into the axoneme. Similarly, the inner arm I1/f 1 $\beta$  HC MTBD was found to be trimethylated on the second Lys of the KK(x)<sub>5</sub>K motif; the unmodified form again was not detected. In contrast, no modifications were identified on the outer arm  $\gamma$  HC MTBD which has the LC1 light chain associated or on the MTBDs of any other inner arm HCs. Within both the  $\alpha$  and  $\beta$  HC MTBDs monomethylation of a single residue on helix H5 (R<sub>3139</sub> and K<sub>3296</sub>, respectively) also occurs; these residues would be oriented almost directly away from the microtubule surface.

**Dynein Methylation is Defective in the *pf22* Cytoplasm.** Although the *Chlamydomonas pf22* strain is a null mutant and does not assemble most dyneins into the axoneme, essentially

wild-type amounts of full-length axonemal dynein HCs are reportedly present in *Chlamydomonas* cytoplasm (24), suggesting that PF22 is not needed for protein folding per se, but rather for some other aspect of holoenzyme formation or maturation. Consequently, we prepared cytoplasmic extracts from the wild-type and *pf22* mutant cytoplasm (Fig. 6A) and additional samples of wild-type axonemes. Following electrophoresis, the dynein HC regions were excised, digested with trypsin or endoproteinase AspN, and subject to tandem MS/MS. The  $\alpha$  and  $\beta$  outer arm HCs are the most heavily modified in wild-type (Table 1) and numerous peptides (>190) were obtained for these proteins from the *pf22* strain. Following extensive analysis of multiple *pf22* gel bands obtained from two different preparations following both tryptic and endoproteinase AspN digestions, we found evidence for only a single low intensity  $\alpha$  HC MTBD-derived methylated peptide DLAAAEPPLVAEAM<sub>ox</sub>AALETVTKK(+me3 on the KK) in one endoproteinase AspN-digested sample. Due to the lack of discriminating fragment ions, we could not distinguish how the methyl groups were distributed on the two Lys residues; four patterns are feasible—K<sub>me3</sub>K, KK<sub>me3</sub>, K<sub>me</sub>K<sub>me2</sub>, or K<sub>me2</sub>K<sub>me</sub>. No methylated peptides derived from any other HCs were identified in *pf22* samples. There were also examples of unmodified HC peptides from *pf22* where the methylated versions in wild-type were readily found (e.g., YVTSQPYDLER<sub>me2</sub> and LDVGEENYAK<sub>me2</sub> from the  $\beta$  HC and FVLFGGCG-R<sub>me</sub> from the  $\alpha$  HC). Similarly, the methylated peptide NTLQQQNEVLCAGR<sub>me</sub> from the IFT dynein was present in the wild-type cytoplasm, but only the unmodified form was found in *pf22*. Thus, the cytoplasm of the *pf22* null mutant appears generally deficient in arginine, but may not be completely lacking lysine, dynein methylase activity.

**Minimal Methyl Modifications on Rat Brain Cytoplasmic Dynein.** We next sought to determine whether methylation is a consistent feature of all dynein HCs or reserved for those involved in cilia formation and function. As *Chlamydomonas* does not encode canonical cytoplasmic dynein, to test whether this major cytoplasmic motor complex is similarly alkylated, we examined the electrophoretically purified HC and ICs of cytoplasmic dynein obtained from rat brain by immunoprecipitation using monoclonal antibody 74-1 (Fig. 6B) (45, 46). For both gel bands, peptide sequence coverage was ~60%. We found evidence for only two monomethylated sites within the rat Dync1h1 protein at R<sub>2394</sub> located in AAA2 and K<sub>4439</sub> in the region C-terminal of AAA6; for both residues, the unmodified peptide intensities were much greater (by 2 to 3 orders of magnitude) suggesting a very substoichiometric level of methylation. In addition, we observed substoichiometric monomethylation on the Dync1i2 IC at K<sub>55</sub> in the extended N-terminal helix, R<sub>455</sub> in a loop connecting two  $\beta$  strands in one WD repeat, and R<sub>629</sub> near the C terminus; for Dync1i1, we identified a single monomethylated Arg (R<sub>467</sub>) located in the WD repeat region. Thus, the regions of rat brain cytoplasmic dynein identified by MS/MS are not methylated in high abundance.

## Discussion

Methylation causes Arg and Lys side chains to become bulkier, more hydrophobic, less capable of H bond formation, and ultimately for trimethyl-Lys residues, unable to form H bonds at all, while still bearing an obligate +1 charge evenly delocalized across four adjacent hydrocarbon groups; in contrast, methylation does not affect salt bridge formation or cation- $\pi$  interactions (*SI Appendix*, Fig. S1). Although protein methylation is perhaps most commonly associated

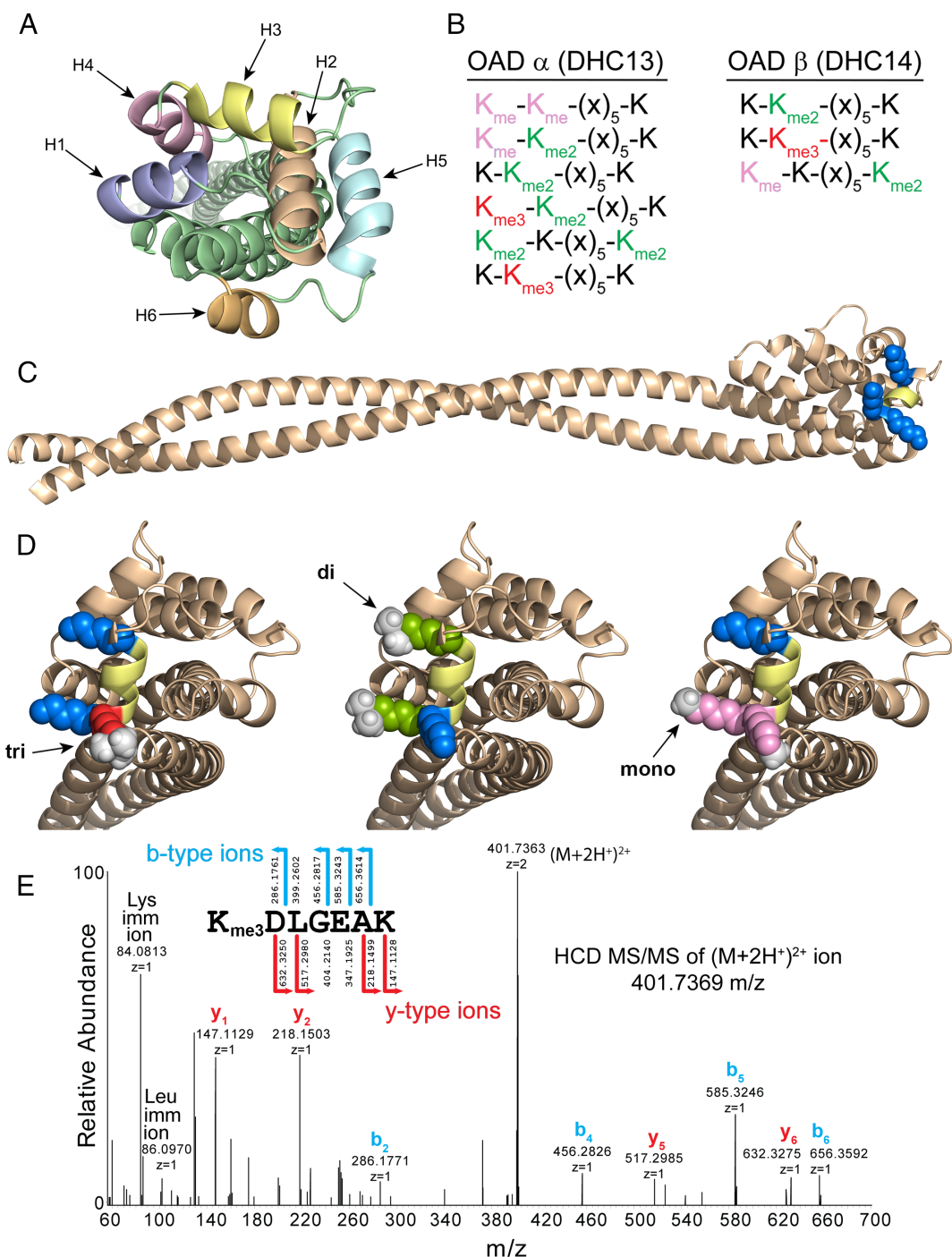


**Fig. 5.** Methylation of microtubule-binding domains. (A) Ribbon diagram of the AlphaFold2 model for the MTBD from the outer arm dynein  $\beta$  HC; the six helices that form this structure are individually colored. (B) Methylation patterns of the MTBD helix H1 KK(x)<sub>5</sub>-K motif as identified by MaxQuant in the paralogous outer arm dynein  $\alpha$  and  $\beta$  HCs. (C) The  $\alpha$  HC MTBD with 2 gyres of the coiled coil (colored wheat). The three Lys residues in the KK(x)<sub>5</sub>-K motif that are variably methylated are shown as space-filling side chains (blue), and the remainder of helix H1 is colored pale yellow. (D) Three of the methylation patterns observed for the  $\alpha$  HC MTBD helix 1: K-K<sub>me3</sub>-(x)-K, K<sub>me2</sub>-K-(x)-K<sub>me2</sub>, and K<sub>me</sub>-K<sub>me</sub>-(x)-K (unmodified, marine blue; monomethylated, pink; dimethylated, split-pea; trimethylated red; methyl groups are in silver/white); these views are related to panel (C) by an ~90° rotation about the vertical axis. (E) Annotated MS/MS spectra and corresponding fragment ion coverage for the tryptic peptide K<sub>me3</sub> DLGEAK from helix 1 of the  $\alpha$  HC MTBD revealing a trimethylated Lys residue at position 2 in the KK(x)<sub>5</sub>-K motif.

with histones and the epigenetic control of transcription (47), these variable and reversible modifications are widespread in biology. For example, methylation occurs on bacterial flagellin and chloroplast Rubisco, is involved in nuclear export of ribonucleoproteins, tumor suppressor activity and apoptosis, conformational control of Hsp90 chaperones, various signaling pathways (including those mediated through MAP Kinase, WNT, and NF- $\kappa$ B), and is also intricately linked to intermediary metabolism through variation in cofactor

availability (see ref. 48 for a comprehensive review). Previous studies of *Chlamydomonas* cilia identified dimethylated Arg residues on several components (49), including radial spoke subunits, tektin, and proteins involved in docking inner arms and the nexin-dynein regulatory complex (50). Furthermore, using antibodies that recognize asymmetric dimethylarginine, methylation status was linked to ciliary disassembly (50, 51), implying that the modifications occurred within cilia. Shortening cilia were also found to have

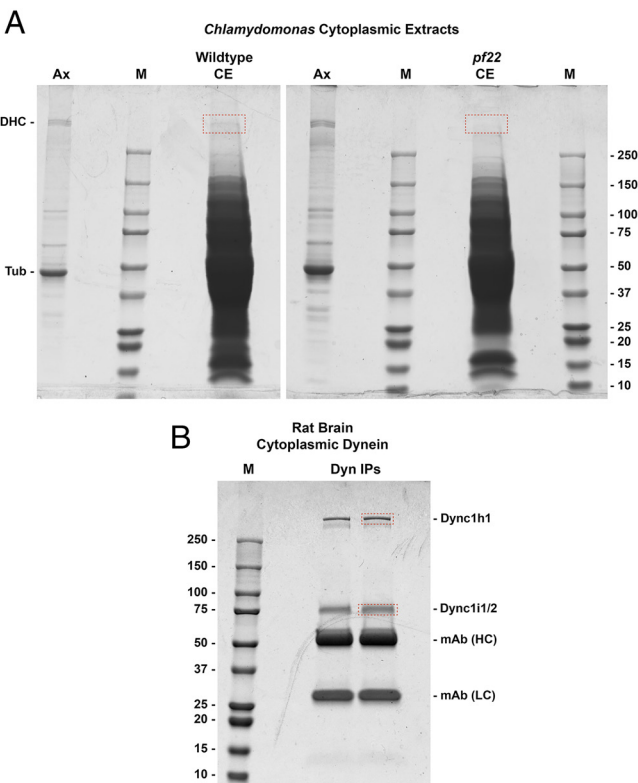


**Fig. 6.** Electrophoretic purification of dyneins from the cytoplasm. (A) Cytoplasmic extracts (lanes labeled CE) from wild-type (CC-125) and *pf22* mutant *Chlamydomonas* cells obtained by multiple rounds of freeze–thaw were electrophoresed in separate gels and stained with Coomassie blue. The dynein HC region was determined using the HC band of wild-type axonemes (Ax) as a marker: DHC, dynein heavy chain; Tub, tubulin. (B) Purified rat brain cytoplasmic dynein HC (Dync1h1) and ICs (Dync1i1/2) were obtained by immunoprecipitation using the 74-1 monoclonal antibody (Dyn IPs) (45) and electrophoresed. The antibody heavy and LCs are indicated by mAb (HC) and mAb (LC), respectively. For all panels, the approximate gel regions excised for MS/MS are indicated by dashed red lines. Molecular weight markers (M) are shown on all panels.

increased levels of the MetE methionine synthase that converts homocysteine to methionine—a precursor of SAM (51).

Here, we identify the axonemal dynein cytoplasmic assembly factor DNAAF3/PF22 as a structural ortholog of SAM-dependent methyltransferases containing the key structural elements essential for enzyme activity. Previous biochemical studies have found that PF22 is exclusively present in the *Chlamydomonas* cytoplasm, and the tagged protein could not be detected in ciliary axonemes (24). This observation is consistent with the complete absence of PF22-derived peptides from numerous independently generated *Chlamydomonas* ciliary proteomes (e.g., refs. 37 and 52 and see the extensive compilation of multiple studies at <http://chlamyfp.org/ChlamyFPv1/index.php>). Thus, any enzymatic and functional activities ascribed to this protein most likely occur in the cytosol. Intriguingly, in *Chlamydomonas* *pf22* mutant cytoplasm, axonemal dynein HCs are present at levels similar to those found in wild-type cells (24), whereas HC levels are depleted in the testes of *Dnaaf3* mutant *Drosophila* (25) suggesting phylogenetic variation in HC stability in the absence of this assembly factor. Furthermore, although we identified dynein HC methylation on both Arg and Lys, in general, methyltransferases usually exhibit specificity for one or other of these basic residues. In *pf22*, we found one example of dynein trimethylation on Lys, but no peptides containing methylated Arg, suggesting that some dynein methylase activity remains in this mutant. Thus, at least one,

currently unidentified, lysine methyltransferase potentially also acts on nascent dynein proteins.

In humans, multiple mutations in DNAAF3 have been directly linked to primary ciliary dyskinesia and classified as pathogenic (24, 53, 54). Several are frameshifts that result in dramatically truncated protein products, while one is a point mutation that changes Leu<sub>61</sub> (in the sequence <sup>59</sup>HLLRT<sub>63</sub>) to Pro (24); note the protein sequence used in refs. 24, 53, and 54 includes 47 additional N-terminal residues that are absent from the current UniProt entry (Q9N9W5). This Leu residue is in helix  $\alpha$ 2 immediately following the Gly-rich loop that forms the base of the SAM-binding pocket. Predictably, converting Leu<sub>61</sub> to Pro would break helix  $\alpha$ 2 one gyre early and likely change the orientation of the Gly-rich loop, thereby affecting SAM substrate binding and leading to altered enzymatic activity. Another mutation (53) converts a buried Val to Glu and may exert a highly destabilizing effect on the entire methyltransferase domain.

Protease sensitivity studies of axonemal dyneins and analysis of HC abundance in *Chlamydomonas* CE (24) suggested that PF22 (DNAAF3) might act at a different, possibly later, stage in the assembly process than do two other factors PF13 (DNAAF2) and ODA7 (DNAAF1), which would be consistent with its serving as a modifying enzyme involved in dynein holoenzyme maturation rather than HC synthesis and folding. In addition, a  $\beta$  HC monoclonal antibody epitope (located between residues 1,129 to 1,168) was hidden in *pf22* cytoplasm but exposed in wild-type; following denaturation and immunoblotting the epitope could be detected in both strains (24). This suggests that loss of PF22 leads to some change in dynein assembly intermediates that hides this  $\beta$  HC epitope which is located in a helical region preceding the linker domain, but methylation appears not to be needed for epitope formation per se. Whether this alteration in assembly state is due to the loss of methyltransferase activity or of a function mediated by the C-terminal inherently disordered region of PF22 (22) remains to be determined; this could be tested by rescuing the *pf22* mutant with a construct encoding a C-terminal truncated version of the protein.

Our mass spectral studies reveal that *Chlamydomonas* axonemal dynein HCs are methylated at multiple sites that depend on the individual motors. Although dynein HCs in general contain upward of 500 or more Arg/Lys residues (Table 1), we found that only a very small subset were methylated. In multiple cases, the equivalent residue in two or more HCs was modified suggesting that particular yet conserved sites are targeted. We found Arg/Lys methylation in three general HC regions including the N-terminal segments involved in particle preassembly, the AAA domain motor unit and on the MTBDs of two outer arm and one inner arm I1/f HCs.

Loss of DNAAF3/PF22 is linked to the failure of some, but not all, dyneins to become integrated within the axonemal superstructure; in *Chlamydomonas*, this includes the outer arms and inner arms b (DHC5), c (DHC9), e (DHC8), and g (DHC7), while the dimeric inner arm I1/f (containing DHC1 and DHC10), and presumably inner arms a (DHC6) and d (DHC2), are still incorporated (17, 24). However, there is not a direct correspondence between methylation status of the ~1,000 residue N-terminal regions involved in motor preassembly and axonemal integration. For example, while the outer arm HCs are methylated at multiple sites within these domains, DHC1, DHC2, and DHC5 are not; yet DHC5 fails to assemble into the axoneme in the absence of PF22. Thus, methylation may not drive axonemal incorporation directly. Potentially, these modifications, perhaps on some more C-terminal HC region, might be required to pass a cytoplasmic licensing event that controls dynein transit into cilia or to enable some intermediate preassembly step (24) to be completed.

Within the AAA domains methylation occurs on residues that are considered key to the ATPase mechanism such as  $\beta$  HC R<sub>1975</sub> that coordinates the acidic residue orienting the water used for hydrolysis in AAA1; the equivalent residue was also modified in the paralogous  $\alpha$  HC supporting a high degree of specificity to this alteration. Additionally, R<sub>2332</sub> that forms the arginine finger derived from AAA2, detecting whether a  $\gamma$ -phosphate is present on the nucleotide in AAA1 and transmitting that information to the adjacent AAA domain is methylated. AAA proteins lacking arginine fingers are generally inactive (40, 41), and altering the biochemical characteristics of this residue will likely impact interdomain connectivity and enzymatic activity. Previous studies fractionating purified outer arm dynein into individual HC subunits revealed that each has a very distinct inherent ATPase activity: 0.6, 7.3, and 1.1  $\mu\text{mol P}_i$  released  $\text{min}^{-1} \text{mg}^{-1}$  for the  $\alpha$ ,  $\beta$ , and  $\gamma$  HCs, respectively (55, 56); it is remarkable that the paralogous  $\alpha$  and  $\beta$  HCs have inherent ATPase rates that differ by an order of magnitude. Furthermore, the separate  $\alpha\beta$  and  $\gamma$  HC outer arm subcomplexes have very distinct pH optima of pH 5.5 (with a second broader peak of activity between pH 7.5 and 9.0) and of pH 10, respectively (57). These observations (reviewed in ref. 58) have never been fully explained, and potentially, differential methylation might impact the ATPase rates and properties of individual motor units when measured using isolated native enzymes.

During the dynein mechanochemical cycle, the MTBD must transition between high- and low-affinity-bound states in response to nucleotide binding and hydrolysis. Furthermore, different dynein HCs have distinct motor properties and translocate microtubules at very different rates in vitro (59). Within the MTBD, high-affinity binding is mediated by helices H2, H3, H4, and H6; the transition to the low-affinity or “off” state occurs when helix H1 is swung forward, pushing against the microtubule surface, and thereby disrupting the tightly bound interface (43, 44). In axonemal dyneins, this helix is partially conserved and contains a variable series of charged residues (see sequence alignment in Dataset S2). The precise makeup of this helix likely dictates the strength of low-affinity associations consistent with the varying in vitro properties of different dyneins (58, 59). For the outer arm  $\alpha$  and  $\beta$  HCs and inner arm I1/f 1 $\beta$  HC, there are three Lys residues in a KK(x)<sub>5</sub>K motif that could interact with the highly acidic microtubule surface. Our observation that this motif is subject to varying patterns of methylation making it bulkier, more hydrophobic, and delocalizing the +1 charges suggests that associations via helix H1 are controlled, potentially fine-tuning the affinity of the loosely bound state. As pf22 axonemes reportedly retain the inner arm I1/f dynein (24), it should be possible to purify both methylated and unmethylated forms of this complex from axonemes of various *Chlamydomonas* strains and compare their enzymatic, microtubule-binding and motor properties directly.

There is considerable variation in the stoichiometry of methylation at different HC sites. For example, although the  $\alpha$  and  $\beta$  HC MTBD helix H1 KK(x)<sub>5</sub>K motifs were found with various patterns of modification, the unmodified forms were not identified. In contrast, the unaltered versions of many other methylated peptides were readily detected and indeed sometimes at intensities considerably greater than the methylated version. As these peptides derived from dyneins already incorporated into the axoneme, we are not identifying intermediate stages in a cytoplasmic pathway leading to fully methylated products. Substoichiometric levels of modification may reflect incomplete DNAAF3/PF22 activity or possibly the action of a dynein demethylase(s) removing certain of these modifications from

some subset of motors. Thus, these extensive differences in modification add an additional level of complexity to the analysis of native dynein proteins because they present as an array of variably methylated types. Whether these variously modified forms occur only on specific MT doublets, occupy particular axonemal locations, or reflect differences in outer arms at distinct positions within the 96 nm axonemal repeat remains to be assessed. Alternatively, random incorporation of these methylated forms with altered mechanochemical properties into the axonemal superstructure might provide inbuilt noise or incoherence to ciliary oscillations that could affect beating coordination, phase slip, frequency drift, or other nonlinear properties.

We also identified a minimal and very substoichiometric set of modifications on rat brain cytoplasmic dynein components suggesting that complex methylation patterns on dynein HCs are likely a defining property of the ciliary motors. This is consistent with the observation that loss of DNAAF3 has no apparent impact on cytoplasmic dynein-mediated processes (24, 25), and indeed canonical cytoplasmic dynein occurs in organisms that do not encode a DNAAF3 ortholog such as the budding yeast *Saccharomyces cerevisiae* and the nematode *Caenorhabditis elegans* (38).

Since the pioneering studies of Ian Gibbons in the 1960s (60), axonemal dyneins from a very broad array of organisms have been extensively analyzed by numerous laboratories. Identification of a conserved assembly factor as a methyltransferase and the presence of multiple methylated sites within axonemal dynein HCs prompts the question of why this modification has not been reported previously. Several factors likely contribute to this, including the general lack and scant use of methylation-specific reagents on ciliary proteins, no obvious driving impetus to impose these variable additions onto prior MS/MS searches, and the substoichiometric nature of many of the modifications. Furthermore, although numerous axonemal dynein structures now have been solved by crystallography and cryo-electron microscopy, none of the electron density maps are of sufficient resolution that methylated side chains would have been readily evident and distinguishable from the unmodified forms; a resolution of ~1.4 Å would likely be needed.

In conclusion, we determine that an essential axonemal dynein assembly factor is a methyltransferase apparently involved in differentially modifying axonemal dynein HCs leading to an array of variously methylated forms. These modifications potentially will have a significant impact on the enzymatic properties of individual dynein particles and illustrate yet more complexity in dynein assembly, single and ensemble motor activity, and the mechanisms of ciliary waveform generation. In the future, it will be important to assess whether axonemal dynein methylation patterns are conserved across a broad array of motile ciliated eukaryotes and to examine the consequences of DNAAF3 loss in other organisms, especially humans.

## Materials and Methods

**Growth of Chlamydomonas Cells.** *C. reinhardtii* wild-type strain CC-125, the outer arm defective strain oda2(CC-2231), and the pf22(CC-2495) null mutant defective for PF22 were obtained from the *Chlamydomonas* Resource Center (<https://www.chlamycollection.org/>). Cells were grown in liquid R medium on a 12 h/12 h light/dark cycle and aerated with 85% air 15% CO<sub>2</sub>. Cells in mid-log phase were harvested by low-speed centrifugation for preparation of cytoplasmic extracts and cilia.

**Preparation of Cytoplasmic Extracts.** Cells were washed with 10 mM Hepes pH 7.4, and cell pellets were immediately frozen at -80 °C. Buffer consisting of 20 mM Tris-Cl pH 8.0, 150 mM NaCl, 5 mM MgSO<sub>4</sub>, 1 mM DTT with protease inhibitor cocktail (P9599; Sigma) was added to the cell pellets and subjected

to three rounds of freeze-thaw by being placed in a  $-80^{\circ}\text{C}$  freezer and frozen cells subsequently warmed to room temperature in a water bath. Samples were then centrifuged at 13,500 rpm at  $4^{\circ}\text{C}$  for 20 min in an AxySpin R centrifuge to pellet cellular debris. The clear supernatants devoid of obvious chlorophyll contamination were mixed with 5× gel sample buffer, heated, and electrophoresed in 4 to 15% TGX polyacrylamide gradient gels (Bio-Rad, Hercules, CA). Following staining with Coomassie blue (Fig. 6A and *SI Appendix*, Fig. S2), the dynein HC region was identified using the HC band of wild-type axonemes as a molecular weight marker, excised, and processed for MS/MS.

**Isolation of Ciliary Axonemes and Dynein HCs.** Cilia were prepared as described in detail previously (61). Briefly, cells in 20 mM Hepes pH 7.4, 5 mM MgSO<sub>4</sub>, and 4% (wt/vol) sucrose (HMS buffer) were deciliated by addition of 7 mM dibucaine-Cl and ~0.003% (wt/vol) CaCl<sub>2</sub>. Cell bodies were removed by differential centrifugation, and the cilia-rich supernatant was overlaid on a 25% sucrose cushion made in 20 mM Hepes pH 7.4 and 5 mM MgSO<sub>4</sub>. Following centrifugation in a ST-8 centrifuge using a swing-out rotor at 2,400 × g for 10 min, cilia were collected from the step gradient interface and pelleted at 30,000 × g at  $4^{\circ}\text{C}$  for 20 min (F21 Fiberlite rotor). For the whole cilia sample, the pellet was resuspended in 20 mM Tris-Cl pH 8.0 and 5% sodium dodecyl sulfate (SDS), immediately frozen at  $-20^{\circ}\text{C}$ , and subsequently processed as described below. Cilia gel samples were prepared by addition of 2× gel sample buffer and electrophoresed in 4 to 15% TGX polyacrylamide gradient gels. Following staining with Coomassie blue (Fig. 3 and *SI Appendix*, Fig. S2), the dynein HC bands were excised and processed for MS/MS.

**Rat Cytoplasmic Dynein.** Cytoplasmic dynein samples were purified from rat brain homogenates by immunoprecipitation with monoclonal antibody 74-1 by the laboratory of Dr. Kevin Pfister (University of Virginia School of Medicine) (45, 46) and kept at  $-80^{\circ}\text{C}$ . These samples were electrophoresed in a 4 to 15% TGX polyacrylamide gradient gel and stained with Coomassie blue (Fig. 6B and *SI Appendix*, Fig. S2). The HC and IC bands were excised, trypsinized, and subject to mass spectral analysis.

**MS/MS.** Coomassie blue-stained gel bands were destained using 40% ethanol and 10% acetic acid in water, diced, equilibrated in 100 mM ammonium bicarbonate pH 8, reduced with 10 mM dithiothreitol in 100 mM ammonium bicarbonate (1 h at  $37^{\circ}\text{C}$ ), and then alkylated with 55 mM iodoacetamide in 100 mM ammonium bicarbonate (45 min at  $37^{\circ}\text{C}$  in the dark). Gel pieces were dehydrated using acetonitrile, dried in a SpeedVac concentrator, and then rehydrated in a 12.5 ng/ $\mu\text{L}$  trypsin solution (Promega porcine sequencing grade trypsin #V5113) in 100 mM ammonium bicarbonate or 12.5 ng/ $\mu\text{L}$  endoproteinase AspN (Roche #V1621). Proteolysis proceeded for 16 h at  $37^{\circ}\text{C}$  on a shaker. Endoproteinase AspN and trypsin-digested peptides were extracted using two sets of alternating washes with 100 mM ammonium bicarbonate and 5% formic acid in 50% acetonitrile followed by two sets of alternating washes with 100 mM ammonium bicarbonate and 100% acetonitrile. Solutions containing extracted peptides were pooled, dried to completion and peptides resuspended in 0.1% formic acid in water.

Whole cilia solubilized in 20 mM Tris-HCl pH 8.0 plus 5% SDS were subjected to sample preparation using S-Trap micro columns (ProFi LLC, Fairport, NY). An aliquot containing 100  $\mu\text{g}$  of total protein was clarified by centrifugation at 14,000 rcf for 5 min, and proteins in the supernatant were subjected to Cys reduction and alkylation using 5 mM dithiothreitol and 20 mM iodoacetamide for 1 h and 30 min in the dark, respectively. Phosphoric acid was added to a final concentration (v/v) of 2.5% after which a 6× volume of binding/wash buffer [100 mM triethylammonium bicarbonate (TEAB) in 90% methanol] was added prior to sample loading onto the S-Trap micro column. The column was then spun at 4,000 rcf for 30 s, and four washes using 150  $\mu\text{L}$  binding/wash buffer were performed with individual 4,000 rcf spins for 30 s each. Protease (Promega sequencing grade trypsin or endoproteinase AspN) in 0.1 M TEAB at a 1:10 (w/w) ratio was added, and digestion was allowed to proceed for 16 h. Proteolyzed peptides were eluted in three consecutive steps using 40  $\mu\text{L}$  aliquots of the following solutions and 4,000 rcf spins of 30 s each: 50 mM TEAB, 0.2% formic acid in water, and 50% acetonitrile in water. Eluted peptides were dried in a SpeedVac concentrator, desalting using Pierce peptide desalting spin columns (P/N 87851) according to the manufacturer's instructions, dried to completion, and resuspended in 0.1% formic acid in water.

Resuspended peptides from gel bands and proteolyzed whole cilia were analyzed using nanoflow ultrahigh performance liquid chromatography (UPLC) coupled to tandem MS/MS using a Dionex Ultimate 3000 RSLCnano UPLC system and Orbitrap Eclipse Tribrid mass spectrometer (ThermoFisher Scientific). Peptides were loaded onto a 75  $\mu\text{m}$  × 25 cm nanoEase m/z Peptide BEH C18 analytical column (Waters Corporation), separated using a 1-h (gel bands) or 2-h (whole cilia) reversed-phase UPLC gradient, and directly ionized into the Orbitrap Eclipse using positive mode electrospray ionization. MS/MS data were acquired using a data-dependent Top15 acquisition method. All raw data were searched against the *Chlamydomonas* proteome database v.5.5 or CC-4532 v.6.1 (<https://phytozome-next.jgi.doe.gov>) using the Andromeda search engine embedded within MaxQuant v.1.6.10.43. Variable modifications included in various searches were Met oxidation, protein N-terminal acetylation, methyl Lys/Arg, dimethyl Lys/Arg, trimethyl Lys, and Ser/Thr/Tyr phosphorylation; carbamidomethylation of Cys was included as a fixed modification. Scaffold v5 (Proteome Software, Inc., Portland, OR) was used for visualization and further analysis.

**Computational Methods.** Model structures for human, rat, mouse, zebrafish, and, in some cases, *Drosophila* dynein assembly factor proteins generated by AlphaFold2 (62) were downloaded from UniProt. As the *Chlamydomonas* models were not available at the time of the initial analysis, these were generated using the Colabfold sever (29), which imposes a 1,000-residue limit, running AlphaFold2. Structural homologs were identified by searching the entirety of the PDB using DALI [<http://ekhidna2.biocenter.helsinki.fi/dali/>] (33). Structures were examined and displayed using the PyMOL molecular graphics system v.2.4.0 (Schrödinger, LLC). Coordinates for proteins structurally related to DNAAF3 were downloaded from the PDB (<https://www.rcsb.org/>) and overlaid on human, zebrafish, and *Chlamydomonas* DNAAF3/Dnaaf3/PF22 using the command "super" within PyMOL to pairwise align C<sub>a</sub> carbons followed by superposition and refinement. Structures of methylated Lys/Arg residues were generated in PyMOL using the "builder" interface.

To determine the location of methylated residues in the *Chlamydomonas* β HC with respect to nucleotide, AlphaFold2 models for AAA1+AAA2, AAA2+AAA3, and AAA3+AAA4 were individually aligned to the human cytoplasmic dynein HC cryo-electron microscopy structure [5NUG; 3.80 Å resolution (39)] which was solved with ADP in AAA1, AAA3 and AAA4, and MgATP in AAA2 using the commands "cealign" and super within PyMOL.

Contrastive machine learning enzyme function prediction from primary sequence (36) for human DNAAF3 and *Chlamydomonas* PF22 was performed at <https://clean.frontend.mml1.ncsa.illinois.edu/configuration>.

The SAM and SAH structures were drawn using ACD ChemSketch. Figures were prepared and annotated using Adobe Illustrator v.27.1.1 and/or Photoshop v.24.1.0.

**Data, Materials, and Software Availability.** Sequence data are available at UniProt <https://www.uniprot.org/> and Phytozome <https://phytozome-next.jgi.doe.gov/>. AlphaFold2 structure predictions for DNAAF3 orthologs are available at UniProt. Cilia proteomic data described in ref. 37 are available at Dryad with the dataset identifier fn2z34txn (63). MS/MS data for whole cilia and dynein HCs from *Chlamydomonas* have been deposited to the ProteomeXchange Consortium <http://proteomecentral.proteomexchange.org/> via the PRIDE partner repository with the dataset identifier PXD045935 (64).

**ACKNOWLEDGMENTS.** We thank Dr. Scott Schafer (University of Massachusetts Medical School) for re-searching the raw data from our previously published cilia proteomes and Dr. Kevin Pfister (University of Virginia School of Medicine) for the cytoplasmic dynein samples. This study was supported by grant R35-GM140631 from the NIH (to S.M.K.). We acknowledge the NIH S10 high-end instrumentation award 1S10-OD028445-01A1, which supported this work by providing funds to acquire the Orbitrap Eclipse Tribrid mass spectrometer housed in the University of Connecticut Proteomics and Metabolomics Facility.

Author affiliations: <sup>a</sup>Department of Molecular Biology and Biophysics, University of Connecticut Health Center, Farmington, CT 06030-3305; and <sup>b</sup>Proteomics and Metabolomics Facility, Center for Open Research Resources & Equipment, University of Connecticut, Storrs, CT 06269

1. S. M. King, *Dyneins: Structure, Biology and Disease. Volume 1-The Biology of Dynein Motors* (Academic Press, Oxford, UK, 2018).
2. J. Lin, D. Nicastro, Asymmetric distribution and spatial switching of dynein activity generates ciliary motility. *Science* **360**, eaar1968 (2018).
3. M. Fliegauf, T. Benzing, H. Omran, When cilia go bad: Cilia defects and ciliopathies. *Nat. Rev. Mol. Cell Biol.* **8**, 880–893 (2007).
4. J. F. Reiter, M. R. Leroux, Genes and molecular pathways underpinning ciliopathies. *Nat. Rev. Mol. Cell Biol.* **18**, 533–547 (2017).
5. A. Shoemark, K. Harman, Primary ciliary dyskinesia. *Sem. Resp. Crit. Care Med.* **42**, 537–548 (2021).
6. Y. Li *et al.*, Global genetic analysis in mice unveils central role for cilia in congenital heart disease. *Nature* **521**, 520–524 (2015).
7. S. M. King, Axonemal protofilament ribbons, DM10 domains and the link to juvenile myoclonic epilepsy. *Cell Motil. Cytoskeleton* **63**, 245–253 (2006).
8. R. J. Faubel *et al.*, Flow blockage disrupts cilia-driven fluid transport in the epileptic brain. *Acta Neuropatholog.* **144**, 691–706 (2022).
9. S. A. Burgess, M. L. Walker, H. Sakakibara, P. J. Knight, K. Oiwa, Dynein structure and power stroke. *Nature* **421**, 715–718 (2003).
10. T. Walton, H. Wu, A. Brown, Structure of a microtubule-bound axonemal dynein. *Nat. Commun.* **12**, 477 (2021).
11. A. P. Carter, C. Cho, L. Jin, R. Vale, Crystal structure of the dynein motor domain. *Science* **331**, 1159–1165 (2011).
12. Q. Rao *et al.*, Structures of outer-arm dynein array on microtubule doublet reveal a motor coordination mechanism. *Nat. Struct. Mol. Biol.* **28**, 799–810 (2021).
13. T. Kon *et al.*, The 2.8 Å crystal structure of the dynein motor domain. *Nature* **484**, 345–350 (2012).
14. A. P. Carter *et al.*, Structure and functional role of dynein's microtubule-binding domain. *Science* **322**, 1691–1695 (2008).
15. A. J. Roberts, T. Kon, P. J. Knight, K. Sutoh, S. A. Burgess, Functions and mechanics of dynein motor proteins. *Nat. Rev. Mol. Cell Biol.* **14**, 713–726 (2013).
16. S. M. King, "Composition and assembly of axonemal dyneins" in *Dyneins: Structure, Biology and Disease. Volume 1-The Biology of Dynein Motors*, S. M. King, Ed. (Elsevier Inc, Oxford, UK, ed. 2, 2018), **vol. 1**, pp. 163–201.
17. D. R. Mitchell, "Cytoplasmic preassembly and trafficking of axonemal dyneins" in *Dyneins: Structure, Biology and Disease. Volume 1-The Biology of Dynein Motors*, S. M. King, Ed. (Elsevier Inc, Oxford, UK, ed. 2, 2018), **vol. 1**, pp. 141–161.
18. D. Nicastro *et al.*, The molecular architecture of axonemes revealed by cryoelectron tomography. *Science* **313**, 944–948 (2006).
19. S. M. King, Cytoplasmic factors for axonemal dynein assembly. *J. Cell Sci.* **134**, jcs258626 (2021).
20. B. Braschi *et al.*, Consensus nomenclature for dyneins and associated assembly factors. *J. Cell Biol.* **221**, e2021109014 (2022).
21. R. L. Huizar *et al.*, A liquid-like organelle at the root of motile ciliopathy. *eLife* **7**, e38497 (2018).
22. S. M. King, Inherently disordered regions of axonemal dynein assembly factors. *Cytoskeleton (Hoboken)*, 10.1002/cm.21789 (2023).
23. E. Hom *et al.*, A unified taxonomy for ciliary dyneins. *Cytoskeleton* **68**, 555–565 (2011).
24. H. M. Mitchison *et al.*, Mutations in axonemal dynein assembly factor DNAAF3 cause primary ciliary dyskinesia. *Nat. Genet.* **44**, 381–389 (2012).
25. P. zur Lage *et al.*, The *Drosophila* orthologue of the primary ciliary dyskinesia-associated gene, DNAAF3, is required for axonemal dynein assembly. *Biol. Open* **10**, bio058812 (2021).
26. B. Huang, G. Piperno, D. J. Luck, Paralyzed flagella mutants of *Chlamydomonas reinhardtii* defective for axonemal doublet microtubule arms. *J. Biol. Chem.* **254**, 3091–3099 (1979).
27. M. Luo, Chemical and biochemical perspectives of protein lysine methylation. *Chem. Rev.* **118**, 6656–6705 (2018).
28. J. Wesche, S. Kühn, B. M. Kessler, M. Salton, A. Wolf, Protein arginine methylation: A prominent modification and its demethylation. *Cell Mol. Life Sci.* **74**, 3305–3315 (2017).
29. M. Mirdita *et al.*, ColabFold: Making protein folding accessible to all. *Nat. Methods* **19**, 679–682 (2022).
30. H. Yamaguchi, T. Oda, M. Kikkawa, H. Takeda, Systematic studies of all PIH proteins in zebrafish reveal their distinct roles in axonemal dynein assembly. *eLife* **7**, e36979 (2018).
31. I. Hanukoglu, Proteopedia: Rossmann fold: A beta-alpha-beta fold at dinucleotide binding sites. *Biochem. Mol. Biol. Educ.* **43**, 206–209 (2015).
32. B. P. S. Chouhan, S. Maimaiti, M. Gade, P. Laurino, Rossmann-fold methyltransferases: Taking a "β-turn" around their cofactor, S-adenosylmethionine. *Biochem* **58**, 166–170 (2019).
33. L. Holm, Dali server: Structural unification of protein families. *Nucl Acid Res.* **50**, W210–W215 (2022).
34. C. Dégut, L. Ponchon, M. Folly-Kian, P. Barraud, C. Tisné, The m1A<sub>58</sub> modification in eubacterial tRNA: An overview of tRNA recognition and mechanism of catalysis by Trm1. *Biophys. Chem.* **210**, 27–34 (2016).
35. M. A. Skiba *et al.*, Biosynthesis of t-butyl in Apratoxin A: Functional analysis and architecture of a PKS loading module. *ACS Chem. Biol.* **13**, 1640–1650 (2018).
36. T. Yu *et al.*, Enzyme function prediction using contrastive learning. *Science* **379**, 1358–1363 (2023).
37. M. Sakato-Antoku, S. M. King, Developmental changes in ciliary composition during gametogenesis in *Chlamydomonas*. *Mol. Biol. Cell* **33**, br10 (2022).
38. B. Wickstead, "The evolutionary biology of dyneins" in *Dyneins: Structure, Biology and Disease. Volume 1-The Biology of Dynein Motors*, S. M. King, Ed. (Elsevier Inc, Oxford, UK, ed. 2, 2018), **vol. 1**, pp. 101–138.
39. K. Zhang *et al.*, Cryo-EM reveals how human cytoplasmic dynein is auto-inhibited and activated. *Cell* **169**, 1303–1314 (2017).
40. A. P. May, S. W. Whiteheart, W. I. Weis, Unraveling the mechanism of the vesicle transport ATPase NSF, the N-ethylmaleimide-sensitive factor. *J. Biol. Chem.* **276**, 21991–21994 (2001).
41. Y. A. Khan, K. I. White, A. T. Brunger, The AAA+ superfamily: A review of the structural and mechanistic principles of these molecular machines. *Crit. Rev. Biochem. Mol. Biol.* **57**, 156–187 (2022).
42. H. Schmidt, E. S. Gleave, A. P. Carter, Insights into dynein motor domain function from a 3.3-Å crystal structure. *Nat. Struct. Mol. Biol.* **19**, 492–497 (2012).
43. S. E. Lacey, S. He, S. H. W. Scheres, A. P. Carter, Cryo-EM of dynein microtubule-binding domains shows how an axonemal dynein distorts the microtubule. *eLife* **8**, e47145 (2019).
44. H. Schmidt, R. Zalyte, L. Urnavicius, A. P. Carter, Structure of human cytoplasmic dynein-2 primed for its power stroke. *Nature* **518**, 435–438 (2015).
45. S. M. King *et al.*, Cytoplasmic dynein contains a family of differentially expressed light chains. *Biochem* **37**, 15033–15041 (1998).
46. J. F. Dillman, K. K. Pfister, Differential phosphorylation *in vivo* of cytoplasmic dynein associated with anterogradely moving organelles. *J. Cell Biol.* **127**, 1671–1681 (1994).
47. E. L. Greer, Y. Shi, Histone methylation: A dynamic mark in health, disease and inheritance. *Nat. Rev. Genet.* **13**, 343–357 (2012).
48. J. Murn, Y. Shi, The winding path of protein methylation research: Milestones and new frontiers. *Nat. Rev. Mol. Cell Biol.* **18**, 517–527 (2017).
49. R. D. Sloboda, L. Howard, Protein methylation in full length *Chlamydomonas* flagella. *Cell Motil.* **66**, 650–660 (2009).
50. R. Werner-Peterson, R. Sloboda, Methylation of structural components of the axoneme occurs during flagellar disassembly. *Biochem* **52**, 8501–8509 (2013).
51. M. J. Schneider, M. Ulland, R. D. Sloboda, A protein methylation pathway in *Chlamydomonas* flagella is active during flagellar resorption. *Mol. Biol. Cell* **19**, 4319–4327 (2008).
52. G. Pazour, N. Agrin, J. Leszyk, G. Witman, Proteomic analysis of a eukaryotic flagellum. *J. Cell Biol.* **170**, 103–113 (2005).
53. F. Wan *et al.*, A novel mutation in PCD-associated gene DNAAF3 causes male infertility due to asthenozoospermia. *J. Cell Mol. Med.* **27**, 3107–3116 (2023).
54. Z. Guo, W. Chen, J. Huang, L. Wang, L. Qian, Clinical and genetic analysis of patients with primary ciliary dyskinesia caused by novel DNAAF3 mutations. *J. Hum. Genet.* **64**, 711–719 (2019).
55. K. K. Pfister, R. B. Fay, G. B. Witman, Purification and polypeptide composition of dynein ATPases from *Chlamydomonas* flagella. *Cell Motil.* **2**, 525–547 (1982).
56. K. K. Pfister, G. B. Witman, Subfractionation of *Chlamydomonas* 18 S dynein into two unique subunits containing ATPase activity. *J. Biol. Chem.* **259**, 12072–12080 (1984).
57. J. L. Gatti, S. M. King, G. B. Witman, "The ATPases of *Chlamydomonas* outer arm dynein differ in their pH and cationic requirements" in *Comparative Spermatology 20 Years After*, B. Baccetti, Eds. (Raven Press, New York, 1991), pp. 373–375.
58. S. M. King, T. Yagi, R. Kamiya, "Axonemal dyneins: Assembly, structure and motor activity" in *The Chlamydomonas Source Book, 3rd Edition. Volume 3: Cell Motility and Behavior*, S. K. Dutcher, Ed. (Elsevier, San Diego, 2023), pp. 79–131.
59. A. Furuta, T. Yagi, H.-a. Yanagisawa, H. Higuchi, R. Kamiya, Systematic comparison of *in vitro* motile properties between *Chlamydomonas* wild-type and mutant outer arm dyneins each lacking one of the three heavy chains. *J. Biol. Chem.* **284**, 5927–5935 (2009).
60. I. R. Gibbons, "Discovery of dynein and its properties: A personal account" in *Dyneins: Structure, Biology and Disease. Volume 1-The Biology of Dynein Motors*, S. M. King, Ed. (Elsevier Inc, Oxford, UK, ed. 2, 2018), **vol. 1**, pp. 5–99.
61. M. Sakato-Antoku, S. M. King, Outer arm dynein light chain LC1 is required for normal motor assembly kinetics, ciliary stability and motility. *Mol. Biol. Cell* **34**, ar75 (2023).
62. J. Jumper *et al.*, Highly accurate protein structure prediction with AlphaFold. *Nature* **596**, 583–589 (2021).
63. S. M. King, M. Sakato-Antoku, Developmental changes in ciliary composition during gametogenesis in *Chlamydomonas*. Dryad. <https://doi.org/10.5061/dryad.fn2z34tn>. Accessed 10 August 2022.
64. M. Sakato-Antoku, R. S. Patel-King, J. L. Balsbaugh, S. M. King, Methylation of ciliary dynein motors involves the essential cytosolic assembly factor DNAAF3/PF22. PRIDE. <https://www.ebi.ac.uk/pride/archive/projects/PXD045935>. Deposited 6 October 2023.